Numerical study of the structural and vibrational properties of amorphous Ta_2O_5 and TiO_2-doped Ta_2O_5

T. Damart,[1] E. Coillet,[1] A. Tanguy,[2] and D. Rodney[1]
[1]*Institut Lumière Matière, UMR 5306 Université Lyon 1-CNRS, Université de Lyon, F-69622 Villeurbanne, France*
[2]*Laboratoire de Mécanique des Contacts et des Structures, UMR 5259 Institut National des Sciences Appliquées de Lyon-CNRS, F-69621 Villeurbanne, France*

(Received 25 February 2016; accepted 23 April 2016; published online 6 May 2016)

Using classical molecular dynamics simulations, we synthesized amorphous Ta_2O_5 and amorphous TiO_2-doped Ta_2O_5. We show that Ta_2O_5 is composed primarily of six-folded Ta atoms forming octahedra that are either organized in chain-like structures or share edges or faces. When Ta_2O_5 is doped with TiO_2, Ti atoms form equally five- and six-folded polyhedra that perturb but do not break the network structure of the glass. Performing a vibrational eigenmode analysis and projecting the eigenmodes on the rocking, stretching, and bending motions of the Ta-2O and Ta-3O bonds, we provide an atomic-scale analysis that substantiates the interpretations of Raman spectra of amorphous Ta_2O_5. This eigenmode analysis also reveals the key role played by Ti atoms in the 5 to 12 THz range. *Published by AIP Publishing*. [http://dx.doi.org/10.1063/1.4948665]

INTRODUCTION

The current quest for the observation of gravitational waves (GW) is opening its second chapter with the first detection of gravitational waves following the start of the advanced Virgo and LIGO detectors.[1,2] The large-scale interferometers at the heart of these detectors use mirrors coated with oxide-based glasses. The coatings are usually multilayers of titanium dioxide doped tantalum pentoxide glasses (Ta_2O_5-TiO_2) and silica (SiO_2). These two materials were chosen because of the contrast between their refractive indices leading to a very large reflectivity. To improve the performance of the detectors, it is however necessary to reduce the thermal noise in the coatings.[3] The origin of this noise is the energy dissipation induced by the internal friction taking place in the amorphous materials.[4,5] Recently, it has been discovered that doping Ta_2O_5 with TiO_2 leads to a reduction of internal friction in the range of frequencies of interest for GW detectors.[6–9] However, the origin of this reduction remains unclear, even if recent works have shown that the medium range order and its change with the addition of Ti play an important role at room temperature.[10] Moreover, while the structure of silica is well-known,[11,12] that of Ta_2O_5 and TiO_2-doped Ta_2O_5 glasses remains unclear. Atomic-scale models have been produced using first-principles,[9] but the systems were small (2000 atoms), and the quench rates used to produce the glasses from the liquid phase were very high (10^{13} K s^{-1}.)

It should also be emphasized that tantalum oxide glasses are of interest outside the field of GW detectors. For instance, they have recently been mixed with alumina to produce extremely strong glasses with excellent optical properties.[13] Tantalum oxides are also traditionally used in electronics due to their electric and dielectric properties.[14]

Our aim here is an in-depth study of the structure and vibrational properties of amorphous Ta_2O_5 and TiO_2-doped Ta_2O_5 glasses produced by molecular dynamics (MD). In order to access large simulation cells allowing for statistical analysis and slow quench rates required to generate relaxed glasses, we represent interatomic bonding using a recently developed interatomic potential.[15] First, the glass structure is characterized in terms of local- and medium-range orders. Second, we present a complete analysis of the vibrational modes of the glasses described with these interactions, and discuss them in relation with current interpretations of Raman spectra.[16–21]

STRUCTURAL CHARACTERIZATION

All simulations were performed using the velocity-Verlet algorithm with a timestep of 1 fs, an Andersen thermostat with a frequency of 1 THz, and periodic boundary conditions (PBC) in all three dimensions. Ta_2O_5 was modeled using a modified van Beest, Kramer, and van Santen (BKS) potential with an extra pseudo-covalent term as proposed by Trinastic *et al.*[15] This modified BKS potential was further optimized using a Wolf truncation to avoid the time-consuming Ewald summation, with the cut-off function proposed by Carre *et al.*[22] and used by Mantisi *et al.*[23] and Koziatek *et al.*[24] to model SiO_2 glasses. Based on the evaluation in Ref. 22, we estimate that, although the present systems are relatively small, we gain about a factor 2 compared to the Ewald summation. After thorough testing, the cut-off radius was set to 15 Å because larger cut-offs lead to similar glass structures. The cut-off of the short-range of the potential was set to 5.5 Å, in order to yield an equilibrium density consistent with experiments, as mentioned later.

We generated 10 samples, cooling a high-temperature liquid at a constant quench rate, followed by energy minimization using quenched dynamics, until the maximum atomic force was below 10^{-4} eV/Å. For the Ta_2O_5 samples, we started from a liquid containing 4711 atoms at 7000 K, which was cooled down to 0 K at constant quench rate. The structure and vibrational properties are only weakly dependent on the

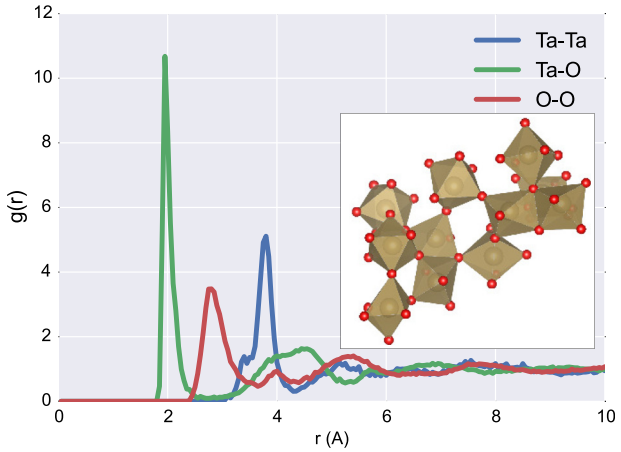

FIG. 1. Pair distribution function in amorphous Ta_2O_5. The inset shows a small section of a sample, with the O atoms in red, and the Ta-centered polyhedra in brown.

quench rate and we will consider here only the lowest rate we tested, 7.10^{11} K/s. During cooling, the cell size was dynamically changed in order to maintain a zero internal pressure. The final density is on average 7.96 g/cm^3 at 0 K, slightly higher than the few experimental densities obtained in thin films, which range from 7.68 g/cm^3 (Ref. 9) to 7.32 g/cm^3 (Ref. 25). However, to our knowledge, no bulk amorphous Ta_2O_5 has ever been synthesized and we are not aware of any measurement in TiO_2-doped Ta_2O_5 glasses. All structural and vibrational analysis were performed after the glasses were relaxed to 0 K by energy minimization.

We first consider the pair distribution function plotted in Fig. 1, which confirms the amorphous structure of the samples. The pair distribution function has a first maximum at 1.92 Å for Ta-O bonds, 3.76 Å for Ta-Ta bonds, and 2.76 Å for O-O bonds. These values agree with those reported in the latest experimental study:[26] from 1.92 to 1.99 Å for Ta-O and from 3.14 to 3.88 Å for Ta-Ta.

Table I presents a nearest-neighbor analysis. In the glass structure, all Ta atoms are surrounded by first-neighbor O atoms. We thus consider here only the Ta-O first-neighbor pairs, defined using the first minimum of the Ta-O pair distribution function. Table I shows that about 70% of the Ta atoms are surrounded by six first-neighbor O atoms, forming Ta-centered octahedra as illustrated in the inset of Fig. 1. There are about 30% Ta atoms with five first-neighbor O atoms, forming bipyramids. The stability of the high Ta-coordination, found in the Ta_2O_5 crystalline structure,[21,27] is due to the pseudo-covalent term added to the BKS potential

TABLE I. Distribution of average coordination numbers in Ta_2O_5. Only the first-neighbor Ta-O bonds are considered.

Tantalum	%	Oxygen	%
Coord. 4	0.5	Coord. 2	69.9
Coord. 5	28.5	Coord. 3	30.1
Coord. 6	69.4		
Coord. 7	1.6		

by Trinastic *et al.*[15] We checked that if this term is removed during quench, tetrahedral networks typical of silica[28] without the higher coordination are obtained.

We note also that about 80% of the octahedra are linked together by a vertex, about 12% share an edge, and 0.5% share a face (two or three oxygens are then shared between two Ta atoms). Examples are seen in the inset of Fig. 1. These structural variations are required by the stoichiometry since a composition of Ta_2O_5 cannot be constructed solely by vertex-sharing octahedra, which would result in a Ta_2O_6 composition. This is different from SiO_2, where the local tetrahedral structure is consistent with the glass stoichiometry, leading to defect-free glasses entirely made of vertex-sharing tetrahedra.

The angular distribution analysis presented in Fig. 2 shows that the inside of each octahedron is ordered, with O-Ta-O angles that are the inter-polyhedra angles, forming either 90° or 180° bonds. The distribution drops to 0° near 180° because of the disappearance of the solid angle in this direction. This artifact can be avoided by biasing the distribution with the sine of the angle, but then the maxima at 90° and 180° are of similar heights, while we expect the maximum at 90° to be higher than at 180° since there are 4 times more 90° angles than 180° angles in an octahedron. The connectivity between octahedra on the other hand is less organized, as shown by the broad distribution of Ta-O-Ta angles that are the inter-polyhedra angles, in Fig. 2(b). We checked that the maximum at 105° is created by O-3Ta (i.e., O atoms with 3 Ta neighbors) and thus the presence of octahedra sharing an edge with one of the local Ta-O bond stretched due the three fold configuration of the O atom. The broad peak between 120° and 180° is formed by O-2Ta and shows that amorphous Ta_2O_5 is a network of interconnected octahedra forming a chain-like structure reminiscent of the structure of crystalline Ta_2O_5.

Using quasistatic simulations, we computed the Young's modulus of Ta_2O_5 and found a value of 146.0 GPa,

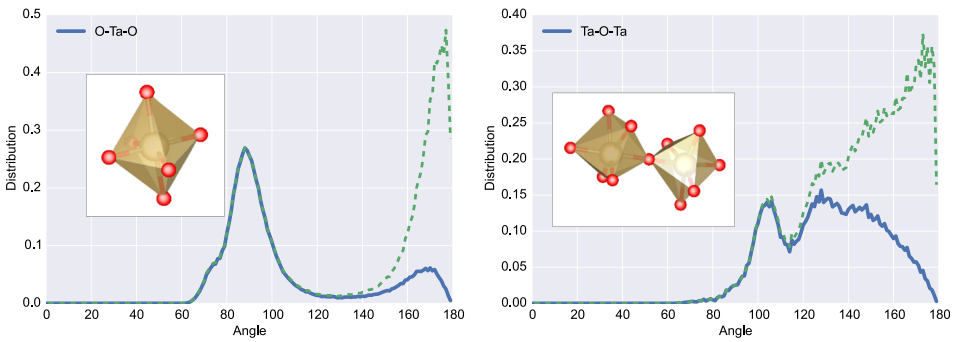

FIG. 2. Angular distribution of bonds in Ta_2O_5: O-Ta-O on the left (intra-polyhedron bonds) and Ta-O-Ta (inter-polyhedron bonds) on the right. The dashed line represents the angular distribution of bonds corrected to take into account the solid angle disappearance at 180°.

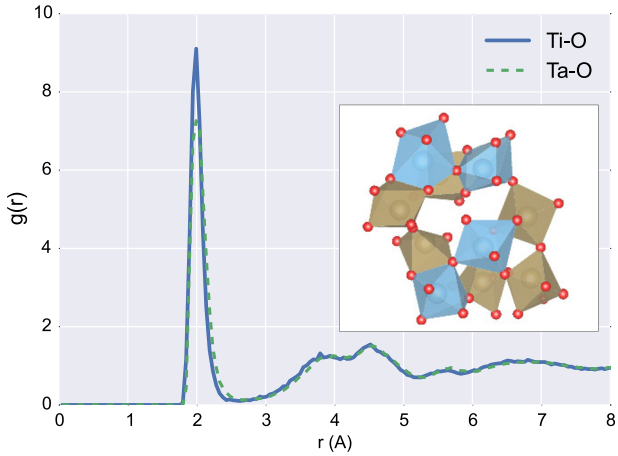

FIG. 3. Ti-O and Ta-O pair distribution functions in Ta_2O_5-TiO_2 (20% Ti). The inset shows a small section of a sample, with the O atoms in red, the Ta-centered polyhedra in brown, and the Ti-centered polyhedra in blue.

close to the experimental value of 140 ± 15 GPa found by nanoindentation of Ta_2O_5 thin films.[29]

The good agreement between the structures generated here and their mechanical properties, with the data provided in the limited experimental literature shows that the present modified BKS potential produces realistic amorphous structures of Ta_2O_5 glasses. We consider Ta_2O_5-TiO_2 using the parameters for the BKS potential optimized by Trinastic *et al.*[15] and noted TiO_{strong}. This choice of parameters leads to five- or six-folded Ti atoms, in agreement with experimental results, which shows that Ti atoms have similar coordinence as Ta atoms in amorphous Ta_2O_5-TiO_2.[30] Following the same approach, we synthesized amorphous samples of Ta_2O_5 doped with 20%, 50%, and 75% of TiO_2 starting from an initial melt of 4700 particles. The following structure and vibrational results will mainly focus on the sample containing 20% of Ti. The glasses obtained after quench have an average density of 8.00 g/cm^3 for a cell size of about 39.0 Å. In Fig. 3, the pair distribution functions show similar profiles for the Ta-O and Ti-O bonds. Considering the representation of the Ta_2O_5-TiO_2 glass in the inset of Fig. 3, we see that the Ti atoms play the same role as Ta atoms, occupying the center of six- and five-folded polyhedra. However, the first peak of the pair distribution function is slightly sharper for Ti-O bonds, indicating that Ti atoms produce a more homogeneous first-neighbor structure, as reported by Bassiri *et al.*[9] The maximum of the pair distribution function is at 1.99 Å for both Ta-O and Ti-O and 3.74 Å for Ta-Ta in agreement with the experimental results reported in Ref. 9. However, the maximum of the pair distribution function is at 3.65 Å for Ti-Ta, which is slightly larger than the experimental value of 3.29 Å. Looking at the number of nearest neighbors in Table II, we see that the environment of the Ta-atoms is not much different from Ta_2O_5 since the fractions of five- and six-folded polyhedra remain close to 30% and 70%, respectively. On the other hand, Ti atoms form almost as many five- and six-fold polyhedra. Also, in Ta_2O_5-TiO_2, more polyhedra share edges and faces, with the consequence that two thirds of the O atoms are three folded, while only one third was three folded in Ta_2O_5.

TABLE II. Distribution of average coordination numbers in Ta_2O_5-TiO_2. Only the first-neighbor Ta-O and Ti-O bonds are considered.

Tantalum	%	Titanium	%	Oxygen	%
Coord. 4	1.1	Coord. 4	4.1	Coord. 2	33.9
Coord. 5	27.6	Coord. 5	45.0	Coord. 3	65.0
Coord. 6	68.7	Coord. 6	50.4	Coord. 4	1.2
Coord. 7	2.6	Coord. 7	0.5		

The bond angle distribution for Ta_2O_5-TiO_2 (Fig. 4) shows an internal organization of the Ta- and Ti-centered polyhedra close to that obtained for Ta_2O_5, with intra-polyhedra angles mainly oriented at 90° and 180°. On the other hand, the distributions are slightly more heterogeneous than in pure Ta_2O_5, since the peaks at 90° and 180° are broader. A dual maximum exists in the O-Ti-O angle distribution around 90°. Fig. 5 represents the angle distribution for Ti-5O and Ti-6O and reveals that the six-folded Ti atoms contribute evenly between 75° and 90° while the five-folded Ti are responsible for the second maximum at 90°. One could expect a peak at 120° as most of the Ti are five-folded; however, a visual inspection of the samples, as the inset of Fig. 5, shows that the oxygens are placed anisotropically around the five-folded Ti atoms in such a way that the O-Ti-O angles are closer to 90° or 180°. The inter-polyhedra Ta-O-Ti, Ta-O-Ta, and Ti-O-Ti angle distributions show two peaks at 100° and 125°. The former was already present in Ta_2O_5 and the latter reflects the shift from 30% of three-folded oxygen atoms in Ta_2O_5 to 60% in Ta_2O_5-TiO_2. Ta_2O_5-TiO_2 glasses retain a structure of network of polyhedra but the higher connectivity of the oxygen atoms implies a structure less close to the chain-like structure of crystalline Ta_2O_5.

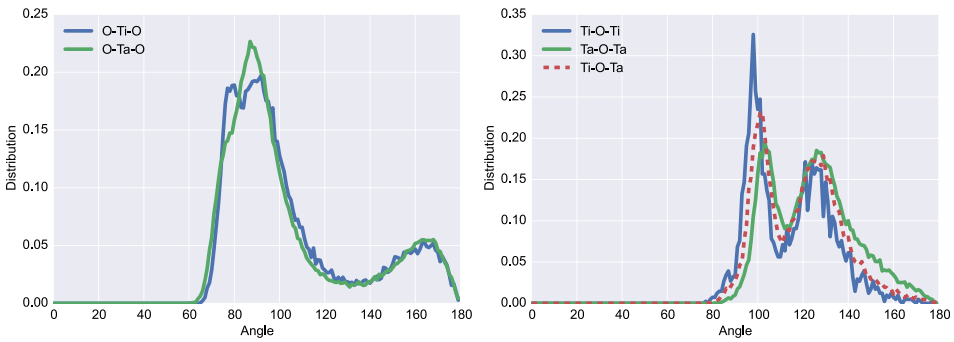

FIG. 4. Angular distribution of bonds in Ta_2O_5-TiO_2 (20% Ti): O-Ta-O and O-Ti-O on the left (intra-polyhedron bonds) and Ta-O-Ta, Ti-O-Ta, and Ti-O-Ti (inter-polyhedron bonds) on the right.

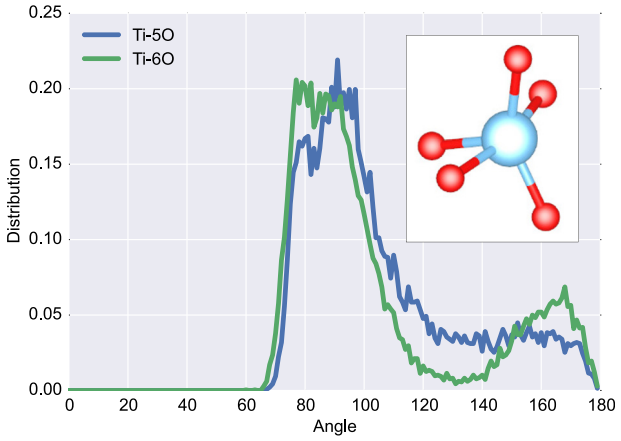

FIG. 5. Angular distribution of bonds for 5- and 6-folded Ti atoms in Ta_2O_5-TiO_2 (20% Ti). The inset shows a Ti-5O cluster with anisotropic placement of the O atoms around Ti. This configuration prevents 120° angles that should be expected from a five-folded atom.

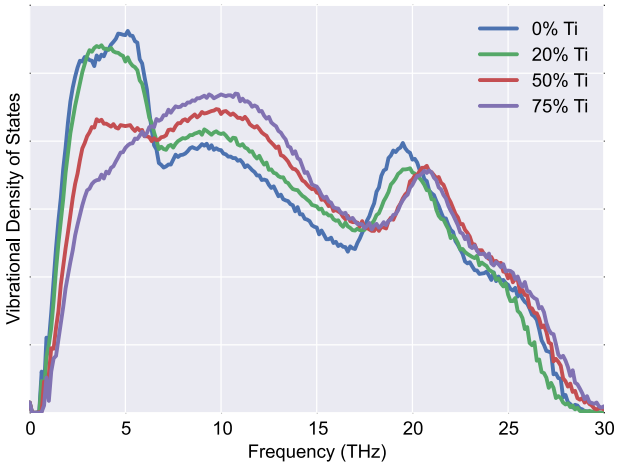

FIG. 7. Vibrational density of states in Ta_2O_5-TiO_2 with different % of Ti atoms.

VIBRATIONAL PROPERTIES

The vibrational response of amorphous Ta_2O_5 and TiO_2-doped Ta_2O_5 glasses has not been reported before. It is important to remind the reader that phonons are not defined in amorphous materials above the Ioffe–Regel limit, where the notion of wavevector becomes ill-defined.[31–33] We will prefer the term of vibration but further categorization is also possible: roton, diffuson, localized modes.[34]

To obtain the vibrational eigenmodes, we compute the dynamical matrix (also referred to as the stiffness or Hessian matrix) by taking the second derivative of the analytical expression of the Wold-truncated modified BKS potential.[35,36] The matrix is defined from the potential energy E_{pot} of the system as

$$D_{ij}^{\alpha\beta} = \frac{1}{\sqrt{m_i m_j}} \frac{\partial^2 E_{pot}}{\partial x_i^\alpha \partial x_j^\beta}, \qquad (1)$$

where i and j refer to particle indices and α and β to directions of space. We performed direct diagonalizations using the LAPACK package.[37] From the diagonalization, we obtained $3N-3$ eigenmodes, the vibrational modes of the system (discarding the 3 translational modes allowed by the PBC), and their $3N-3$ corresponding eigenvalues, which are the square of the vibrational frequencies (N is the number of particle in the system). Plotting the frequency distribution of these modes for Ta_2O_5 and Ta_2O_5-TiO_2, we obtain the vibrational density of state (VDOS) presented in Fig. 6. In addition, we plot partial VDOS, which represent the weighted displacements carried by Ta, Ti, or O atoms, and is defined as

$$VDOS(\omega) = \frac{1}{3N-3} \sum_i^M \sum_n^{3N-3} |u_i^n|^2 \delta(\omega - \omega_n), \qquad (2)$$

where u_i^n is the displacement of the i-th particle in the nth mode restricted to i being either Ta, Ti, or O atoms, and M the number of the corresponding type of atoms. As seen in Fig. 6, for Ta_2O_5, the Ta atoms are the main carriers of vibrations at low frequencies ($<6 \sim 7$ THz), while the O atoms are dominant at higher frequencies. This is coherent with the difference of mass between Ta (heavier) and O atoms. In Ta_2O_5-TiO_2, the Ti particles carry the displacements around 8.5 THz, which is between the Ta- and O-dominated ranges of frequencies. Fig. 7 shows the evolution of the VDOS for different Ti compositions. As expected from the partial VDOS in Fig. 6, when the % of Ti atoms increases, the first peak, which arises from the Ta atom vibrations, decreases while the presence of additional Ti atoms adds frequencies between 5 and 15 THz. Also, the O peak at 19 THz is slightly shifted toward higher frequencies.

To characterize the vibrational eigenmodes, we computed the participation ratio (PR), which expresses the fraction of the particles in the system that takes part into the motion for a given mode. The PR is defined as

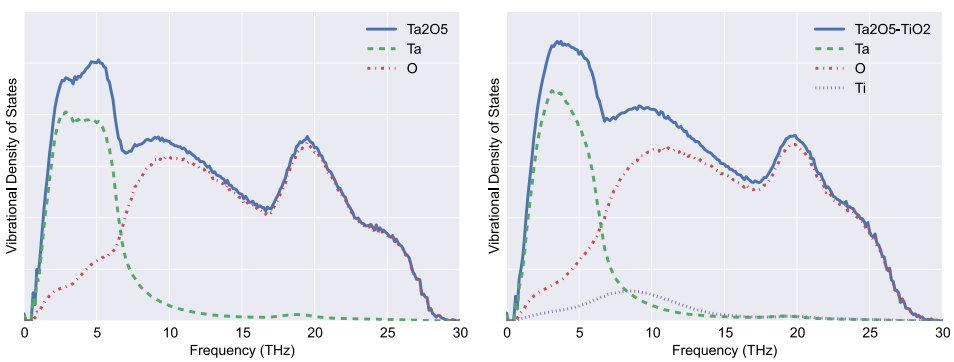

FIG. 6. Full and partial vibrational density of states in Ta_2O_5 (left) and Ta_2O_5-TiO_2 (20% Ti) (right).

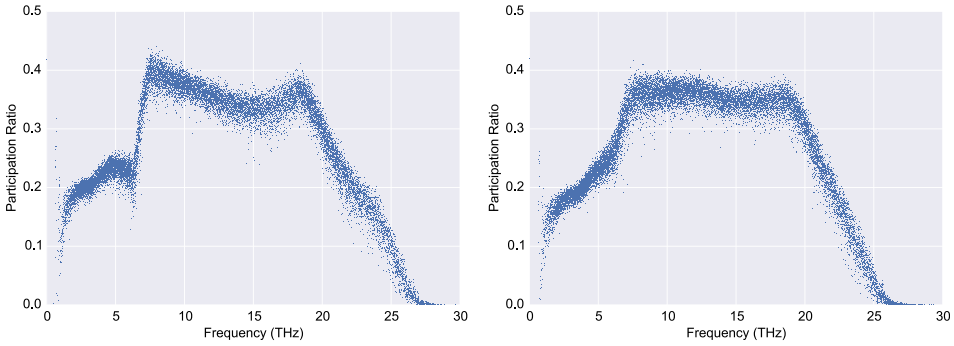

FIG. 8. Participation ratio in Ta_2O_5 (left) and Ta_2O_5-TiO_2 (20% Ti) (right). Each dot represents an eigenmode.

$$PR(\omega) = \frac{1}{N} \frac{\left(\sum_{i=1}^{N} \|\vec{u}_i^n\|^2 \right)^2}{\sum_{i=1}^{N} \|\vec{u}_i^n\|^4} \delta(\omega - \omega_n). \quad (3)$$

For Ta_2O_5, the PR plotted in Fig. 8 shows four different regimes: (1) From 0 to 2 THz, there is a mix of high PR, delocalized, modes and low PR modes that correspond to soft modes. The delocalized modes are plane waves spanning the entire system and leading to a wavelength-dependent high PR. Soft modes are the superposition of delocalized modes of long wavelength with localized displacements involving only small selected groups of particles. These modes are known to be the markers of imminent plastic deformation (their frequency tends to zero when the system approaches a plastic event).[38–40](2) From 2 to 6 THz, the PR increases slowly from 20% to 25% before dropping down to 14% at 6.5 THz. This region is dominated by the Ta vibrations and the relatively low PR is due to the fact that Ta atoms represent only 2/7th of the total number of atoms. The drop in PR corresponds to the crossover frequency between Ta- and O-dominated vibrations (See Fig. 6), a frequency range where neither the Ta nor the O can carry vibrations. (3) From 6 to 19 THz, there is a plateau between 30% and 40% with some modes going as low as 24%. This regime matches the frequency range where the O atoms carry the vibrations. (4) From 19 to 30 THz, the PR shows a continuous decay down to 0% at about 30 THz, corresponding to modes more and more spatially focused. These high-frequency modes are equivalent to optic modes in crystalline materials.[41]

Looking at the PR for Ta_2O_5-TiO_2, we see that the TiO_2 doping removes the drop previously observed at 6 THz. The reason is that, as seen in the partial VDOS of Fig. 6, the Ti atoms fill the vibrational gap in this frequency range. No other significant differences are observed between the Ta_2O_5 and Ta_2O_5-TiO_2 spectra.

We plot in Fig. 10 the partial VDOS for O atoms projected on the rocking, stretching, and bending motions illustrated in Fig. 9. For the two folded oxygens, the motion of the oxygen atom for each mode is projected on three different vectors as in Refs. 42 and 43. For the three folded oxygens, bond bending is obtained by projecting the motion of the O atom on a unit vector perpendicular to the plane of the three Ta neighbors, while the remaining part of the motion is an in-plane vibration, which corresponds to the stretching of the bond. We did not find an equivalent of rocking motion of a O-3Ta bond.

In the absence of experimental data for the VDOS of glassy Ta_2O_5, we compare our calculations with experimental Raman data. It should be noted that most interpretations of Raman data[16–21] are based on an analogy of other oxide compounds due to the limited knowledge available on the structure of amorphous Ta_2O_5. The present Raman measurements were performed on a 15 μm thick glassy Ta_2O_5 layer deposited through ion beam sputtering. Spectra were recorded at room temperature with a confocal LabRAM HR Evolution micro-spectrometer. Measurements were carried out using a YAG:Nd3 + laser line at 532 nm, from 5 to 1500 cm^{-1} with a 2.5 mW laser power at focal point. A confocal pinhole diameter was set at 75 μm allowing to probe

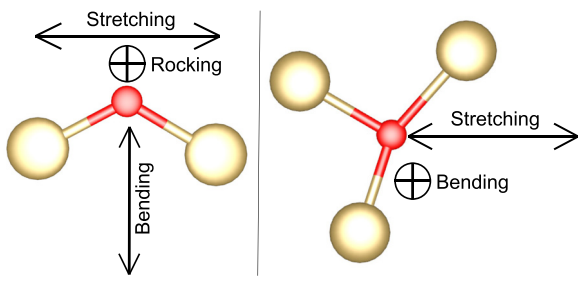

FIG. 9. Sketch of O-2Ta and O-3Ta bonds with the vectors used to decompose the bond deformation into bending, stretching, and rocking components.

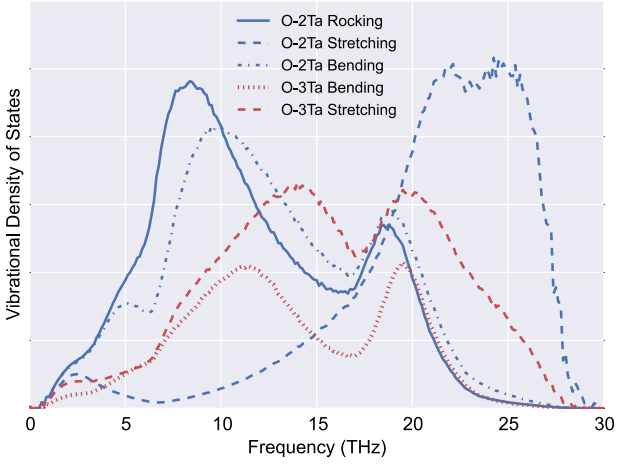

FIG. 10. Decomposition of the vibrational density of states in a Ta_2O_5 glass onto the rocking, stretching, and bending of O-2Ta bonds, and on the bending and stretching of O-3Ta bonds.

only the thin layer. Fig. 11 compares the computed VDOS with the experimental reduced Raman intensity (i.e., the measured intensity divided by the thermal population factor $n(\omega,T)+1$ for Stokes scattering). Although the Raman response provides an indirect picture of the VDOS (through polarizability modulation), the two curves show good qualitative agreement in terms of their main features and respective intensities.

The most prominent feature seen in the Raman spectrum of Fig. 11 is the band at 20 THz ($\sim$670 cm^{-1}). This band is present in the partial VDOS of Fig. 10 at this same frequency and corresponds to maxima for both O-3Ta bending and stretching, which agrees with former interpretations of Raman spectra.[16,17,19] At higher frequencies, above 24 THz ($\sim$800 cm^{-1}), the Raman spectrum shows a shoulder, also present in the calculated VDOS albeit less extended toward the high frequency end. According to the partial VDOS of Fig. 10, this shoulder is due to the stretching of O-2Ta, which is again in agreement with the literature.[16,17,19]

Below 7 THz ($\sim$230 cm^{-1}), the Raman spectrum essentially consists of a sharp band peaking at 2 THz ($\sim$70 cm^{-1}), while in this frequency range the calculated VDOS shows a wider dual maximum. The accepted interpretation of the Raman band below 3 THz is that the vibrations arise from inter-polyhedra interactions or/and charged clusters.[17–20] However, Fig. 6 shows that from 0 to 5 THz, the vibrations are essentially carried by the Ta atoms that can be viewed as optical-like modes lying in the low frequency range due to the large mass of the Ta atoms. This is confirmed by the observation of low frequency narrow bands in the Raman spectra of crystalline Ta_2O_5.[20] Therefore, the sharp band observed in the low frequency Raman spectrum of Ta_2O_5 does not seem to be linked to inter-polyhedra interactions. Note that the absence of a double band in the Raman spectrum, unlike the VDOS, can be due to polarization effects (i.e., Raman selection rules) not accounted for in the VDOS calculations. It is worth mentioning that the low frequency range near 2 THz ($\sim$70 cm^{-1}) is typical for the excess VDOS (or boson peak) for inorganic glasses. Due to the low-lying optical-like vibrations of the heavy Ta atoms, it is impossible to clearly identify a boson peak for Ta_2O_5 though it may lie underneath the low frequency bands. A clarification of this matter would require to investigate lower frequency vibrations (i.e., below 0.5 THz), which is not possible with the present calculations due to the limited box size of the samples. Note that the slight discrepancy between the VDOS and the Raman curves observed toward the lowest frequency edge below 2 THz can also be due to the presence of quasielastic scattering in the Raman signal, which is ascribed to anharmonic motions that are not modeled by our calculations.

Finally, from 3 to 13 THz ($\sim$100–430 cm^{-1}), the Raman spectrum shows a shoulder also seen in the VDOS, although at slightly larger frequencies. The Raman band at these frequencies is usually explained by internal O-Ta-O bending, as is the case in similar oxides at these frequencies.[17] The partial VDOS plotted in Fig. 10 shows that most of the vibrations in this frequency range are indeed carried by the bending and rocking motions of O-2Ta, thus in agreement with the Raman interpretation.

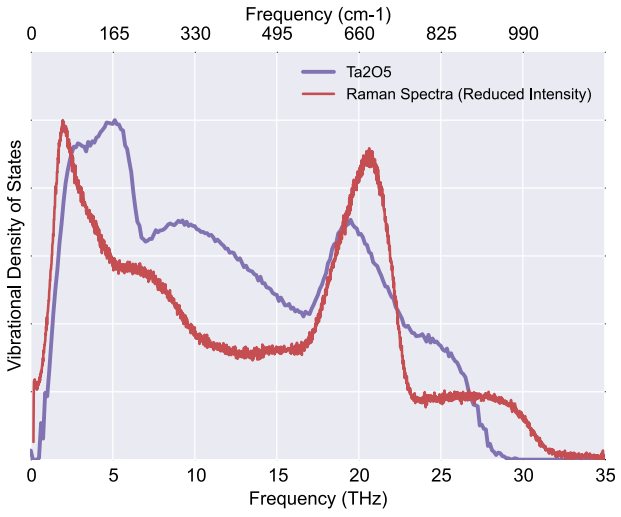

FIG. 11. Full vibrational density of states in Ta_2O_5 (in blue) superimposed with the Raman spectra of Ta_2O_5 (in red).

CONCLUSION

We used classical molecular dynamics simulations to study the structure of amorphous Ta_2O_5 and amorphous TiO_2 doped Ta_2O_5. We showed that these materials are formed of chains of octahedra linked by a vertex, an edge, or a face. We also showed that doping amorphous Ta_2O_5 with TiO_2 does not alter the glass structure in a strong way. Performing an eigenmode analysis we showed a good agreement between our spectra and Raman measurement. And projecting the eigenmodes on either the atomic type, or the rocking, stretching, and bending motions, we discussed the accepted interpretation of Raman measurements. In the future, it would be interesting to use a more extended model to investigate the low-frequency vibrations that could arise from interactions between ionic clusters, especially to look at larger system sizes. Also, in this work we have considered the THz frequency range of interest for Raman spectroscopy used to characterize the short- and medium-range orders in glasses. Internal friction for applications in gravitational wave detectors mentioned in the Introduction section occurs in the Hz to kHz regime, where dissipation mechanisms are different from the THz regime. This aspect has been recently explored numerically in Refs. 10 and 44.

ACKNOWLEDGMENTS

T.D. and D.R. acknowledge support from LABEX iMUST (ANR-10-LABX-0064) of Université de Lyon (program "Investissements d'Avenir," ANR-11-IDEX-0007). Stimulating discussions with Professor Gianpietro Cagnoli, Professor Alain Mermet, and Professor Valérie Martinez are also gratefully acknowledged.

[1]B. P. Abbott *et al.*, Phys. Rev. Lett. **116**, 061102 (2016).
[2]M. Adier, F. Aguilar, T. Akutsu, and M. Arain, Gen. Relativ. Gravitation **46**, 1749 (2014).
[3]T. Hong, H. Yang, E. K. Gustafson, R. X. Adhikari, and Y. Chen, Phys. Rev. D **87**, 082001 (2013).

[4]R. Kubo, Rep. Prog. Phys. **29**, 255 (1966).
[5]H. Nyquist, Phys. Rev. **32**, 110 (1928).
[6]I. Martin, E. Chalkley, R. Nawrodt, H. Armandula, R. Bassiri, C. Comtet, M. Fejer, A. Gretarsson, G. Harry, D. Heinert *et al.*, Classical Quantum Gravity **26**, 155012 (2009).
[7]C. Comtet, D. Forest, P. Ganau, G. M. Harry, C. Michel, N. Morgado, V. Pierro, and L. Pinard, paper presented at the 42th Rencontres de Moriond-Gravitational Waves and Experimental Gravity, La Thuile, Italy (2007).
[8]M. Granata, K. Craig, G. Cagnoli, C. Carcy, J. Degallaix, R. Flaminio, D. Forest, J.-S. Hennig, J. Hough, I. Maclaren *et al.*, Opt. Lett. **38**, 5268 (2013).
[9]R. Bassiri, K. Evans, K. B. Borisenko, M. M. Fejer, J. Hough, I. Maclaren, I. W. Martin, R. K. Route, and S. Rowan, Acta Mater. **61**, 1070 (2013).
[10]J. P. Trinastic, R. Hamdan, C. Billman, and H.-P. Cheng, Phys. Rev. B **93**, 014105 (2016).
[11]A. N. Cormack and Y. Cao, Mol. Eng. **6**, 183 (1996).
[12]S. Sugai and A. Onodera, Phys. Rev. Lett. **77**, 4210 (1996).
[13]G. A. Rosales-Sosa, A. Masuno, Y. Higo, H. Inoue, Y. Yanaba, T. Mizoguchi, T. Umada, K. Okamura, K. Kato, and Y. Watanabe, Sci. Rep. **5**, 15233 (2015).
[14]J. Lin, N. Masaaki, A. Tsukune, and M. Yamada, Appl. Phys. Lett. **74**, 2370 (1999).
[15]J. P. Trinastic, R. Hamdan, Y. Wu, L. Zhang, and H. Cheng, J. Chem. Phys. **139**, 154506 (2013).
[16]J. Meng, B. K. Rai, R. Katiyar, and A. S. Bhalla, J. Phys. Chem. Solids **58**, 1503 (1997).
[17]P. S. Dobal, R. S. Katiyar, Y. Jiang, R. Guo, and A. S. Bhalla, J. Raman Spectrosc. **31**, 1061 (2000).
[18]P. S. Dobal, R. S. Katiyar, Y. Jiang, R. Guo, and A. S. Bhalla, J. Appl. Phys. **87**, 8688 (2000).
[19]H. Ono, Y. Hosokawa, K. Shinoda, K. Koyanagi, and H. Yamaguchi, Thin Solid Films **381**, 57 (2001).
[20]C. Joseph, P. Bourson, and M. D. Fontana, J. Raman Spectrosc. **43**, 1146 (2012).
[21]Q. Li, H. Zhang, B. Cheng, R. Liu, B. Liu, J. Liu, Z. Chen, B. Zou, T. Cui, and B. Liu, J. Appl. Phys. **115**, 193512 (2014).
[22]A. Carre, L. Berthier, J. Horbach, S. Ispas, and W. Kob, J. Chem. Phys. **127**, 114512 (2007).
[23]B. Mantisi, A. Tanguy, G. Kermouche, and E. Barthel, Eur. Phys. J. B **85**, 304 (2012).
[24]P. Koziatek, J. Barrat, and D. Rodney, J. Non-Cryst. Solids **414**, 7 (2015).
[25]T. Li, F. A. A. Sandoval, M. Geitner, L. Bellon, G. Cagnoli, V. Dolique, R. Flaminio, M. Granata, C. Michel, N. Morgado *et al.*, Phys. Rev. D **89**, 092004 (2014).
[26]R. Bassiri, F. Liou, M. R. Abernathy, A. C. Lin, N. Kim, A. Mehta, B. Shyam, R. L. Byer, E. K. Gustafson, M. Hart *et al.*, APL Mater. **3**, 036103 (2015).
[27]R. Hollerweger, D. Holec, J. Paulitsch, M. Bartosik, R. Daniel, R. Rachbauer, P. Polcik, J. Keckes, C. Krywka, H. Euchner *et al.*, Acta Mater. **83**, 276 (2015).
[28]K. Vollmayr, W. Kob, and K. Binder, Phys. Rev. B **54**, 15808 (1996).
[29]G. Alaca, P. Skeldon, G. E. Thompson, A. B. Mann, H. Habazaki, and K. Shimizu, Nanotechnology **13**, 451 (2002).
[30]R. Bassiri, M. R. Abernathy, F. Liou, A. Mehta, E. K. Gustafson, M. J. Hart, N. Kim, A. C. Lin, I. Maclaren, I. W. Martin *et al.*, J. Non-Cryst. Solids **438**, 59 (2016).
[31]Y. M. Beltukov, V. I. Kozub, and D. A. Parshin, Phys. Rev. B **87**, 134203 (2013).
[32]Y. M. Beltukov, C. Fusco, D. A. Parshin, and A. Tanguy, Phys. Rev. E **93**, 023006 (2016).
[33]T. Damart, V. M. Giordano, and A. Tanguy, Phys. Rev. B **92**, 094201 (2015).
[34]P. Allen and J. Feldman, Philos. Mag. B **79**, 1715 (1999).
[35]M. Dove, Éc. Thématique de la Soc. Fr. Neutronique **12**, 123 (2011).
[36]N. W. Ashcroft and N. D. Mermin, *Solid State Physics* (Brooks Cole, 1976).
[37]See http://www.netlib.org/lapack/ for Linear Algebra PACKage.
[38]A. Tanguy, B. Mantisi, and M. Tsamados, Europhys. Lett. **90**, 16004 (2010).
[39]M. L. Manning and A. J. Liu, Phys. Rev. Lett. **107**, 108302 (2011).
[40]J. Rottler, S. S. Schoenholz, and A. J. Liu, Phys. Rev. E **89**, 042304 (2014).
[41]M. Marinov and N. Zotov, Phys. Rev. B **55**, 2938 (1997).
[42]S. N. Taraskin and S. R. Elliott, Phys. Rev. B **56**, 8605 (1997).
[43]N. S. Shcheblanov, B. Mantisi, P. Umari, and A. Tanguy, e-print arXiv:1502.00898v1.
[44]R. Hamdan, J. Trinastic, and H. Cheng, J. Chem. Phys. **141**, 054501 (2014).